*Netherlands Journal of Agricultural Science 45 (1997) 127-142*

# Modelling and simulation for control of nutrient application in closed growing systems

T.H. GIELING[1,*], J. BONTSEMA[1], T.W.B.M. BOUWMANS[2] AND R.H. STEEGHS[2]

[1] Institute of Environmental and Agricultural Engineering (IMAG-DLO), P.O.Box 43, NL-6700 AA Wageningen, The Netherlands
[2] Department of Agricultural Engineering and Physics, Wageningen Agricultural University, Bomenweg 4, NL-6703 HD Wageningen, The Netherlands
* Corresponding author (fax:+31-317-425670; e-mail: th.h.gieling@imag.dlo.nl)

Received 23 September 1996; accepted 21 February 1997

## Abstract

In some European countries the year 2000 will be a target to enforce the use of closed growing systems in greenhouses. Closed growing systems collect the surplus of water and nutrients and recirculate it to the crop after treatment. The design of a controller for water supply and nutrient application in closed growing systems is presented and discussed.

Seasonal changes in the root mat or models which do not describe the real process precisely in all details, influence the general stability of the controlled supply process. It is shown, that robust performance and robust stability – as qualities of the controlled process – are feasible in these circumstances. Loopshaping proves to be a very useful design technique. Algorithm performance is tested in a simulation procedure. Results of simulation tests show very good disturbance suppression.

*Keywords:* closed growing system, nutrient application, robust control, loopshaping

## Introduction

Development of soilless growing systems on a commercial scale in protected cultivation already started in the early eighties. Higher production, energy saving, stopping the spread of soil-born pathogens and a better control of growth and quality were the reasons for changing. Problems which had to be tackled were the particular layout of the growing system, the kind and size of the substrate, the capacity, layout and make of the water supply system, the high root temperature and the control of electrical conductivity (EC), pH and nutrient composition of the solution. Practical experience with open systems showed that a water surplus of 30% is needed to wash the remaining nutrient salts out of the substrate. The surplus of water and fertilisers simply flushed into the subsoil. It was not considered to be a problem until a general awareness did arise concerning the polluting effects of fertilisers to ground- and surface water.

Nowadays, commercially available equipment for water and nutrient supply uses classic analogue or digital P, PI and PID controllers. In so called A/B type of systems, A or B type of solute mixtures are subsequently added into a mixing tank. These diluters add the solute in relation to the EC value measured in the supplied nutrient solution. The pH value of nutrient supply is kept within the range of approximately 5.5–6.5.

Most commercially available systems show problems in compensating relatively fast changes of the nutrient uptake, the stock solutions or – in case of closed growing systems – the drain water returning from the plants (Kupers *et al.*, 1992). Only recently some publications on new strategies for system identification and new algorithms for control of water and nutrient application were presented, where the feedback of ion selective measurements is considered in the control of the application of individual ions.

Hashimoto *et al.* (1989) used ion selective sensors to study and elucidate the dynamic characteristics of nutrient uptake. They propose the application of fuzzy logic and a neural network to control water and nutrient supply and the pH level of a 'deep flow' hydroponic growing system.

True digital control of a nutrient film technique (NFT) system with top-end water supply is described by Young *et al.* (1991), Chotai & Young (1991) and Chotai *et al.* (1991). They suggest a self adaptive and self tuning control method for systems whose dynamic characteristics change over time. Their papers report on the development of an adaptive control approach with a Proportional Integral Plus controller.

Honjo & Takakura (1991) suggest the use of a simple neural net structure for the identification of water and nutrient supply to a hydroponic tomato plant growing system. By using 8 hours of input data from 5 environmental factors and a neural net with one hidden layer (4 nodes), the amount of water and nutrient supply is calculated from the time series of these 5 environmental factors.

Okuya & Okuya (1991) report on an ion controlled feeding method for hydroponics, based on the calculation of the nutrient ions absorbed by the crop. Depending on the value of EC, the adding ratio of one out of four kinds of stock solute was calculated on the basis of the absorbed concentration of each ion.

It is the aim of the research project described in the paper at hand, to develop a multivariable controller for the application of water and eight macro nutrients. It separately injects liquid nutrients by means of a nutrient dispenser in the main stream of a closed, recirculating trickle irrigation water supply system. This paper explains a design method for a controller where a SISO (single-input single-output) system is taken as an example. The concentration of the potassium ion is measured. The controller is intended to keep the amount of potassium ($mol \cdot s^{-1}$) returning from the plants at a constant level. The design method – taken from standard control engineering theory – results in a controller with robust performance and stability properties. In relation to nutrient supply this means in general, that the controlled process remains stable and within chosen allowable margins, in spite of uncertainties in the process models (i.e. seasonal changes in the root mat or models which do not describe the real process precisely in all details). The controller compensates disturbances caused by the nutrient uptake of the plants. The paper describes the use of the

technique of loopshaping, where Bode plots enable well defined choices to determine the properties of the controller.

## Materials and methods

*General layout of the supply system*

The nutrient supply system is situated in a 150m$^2$ greenhouse with a NFT closed growing system and eight rows of tomato plants in gullies, each gully covered with a lid. Seedlings stay in 10×10×10 cm rockwool seedling blocks. Water is supplied by means of a trickle irrigation system. The layout of the water supply system follows the Tichelmann design (Figure 1). In a Tichelmann system an extra pump circulates the nutrient solution through the supply pipes in order to reduce the dead time of nutrient supply (Gieling *et al.*, 1994). The drain water from the gullies is collected in a small return pit below the surface of the greenhouse floor and pumped into a mixing tank. The nutrient solution in the mixing tank is kept at the standard nutrient concentration by means of an A/B diluter system. In the A/B solutes the $K^+$ is kept at a low value (Figure 1), in order to allow for a separately controlled injection of $K^+$. The potassium concentration is measured in the return pit, using an analyser with ISFET sensors (Gieling *et al.*, 1996). A flow controlled pump injects potassium – e.g. as

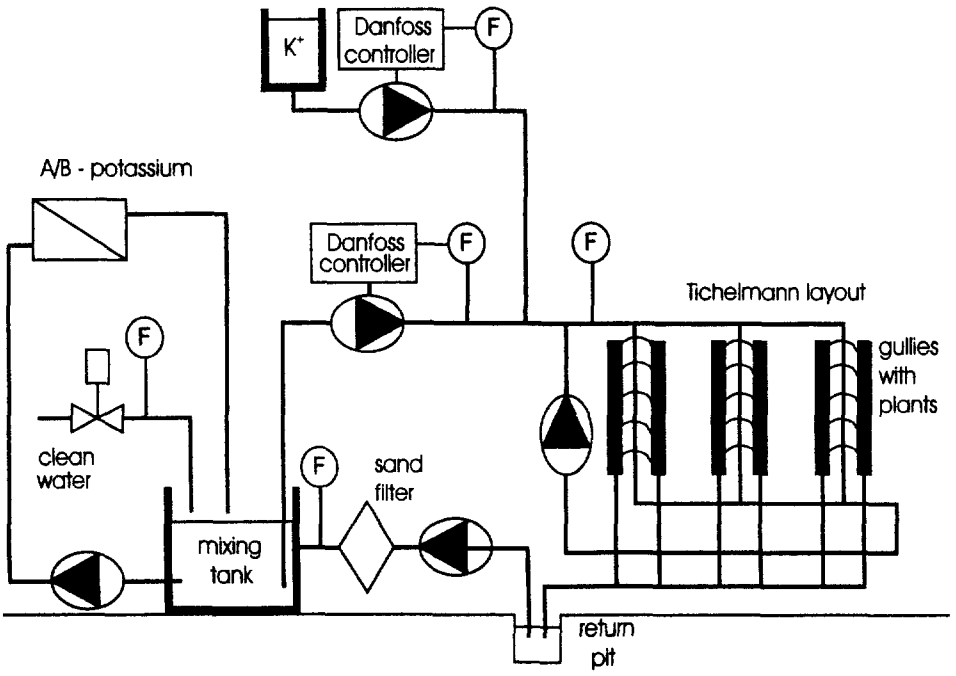


Figure 1. Layout of the supply system.

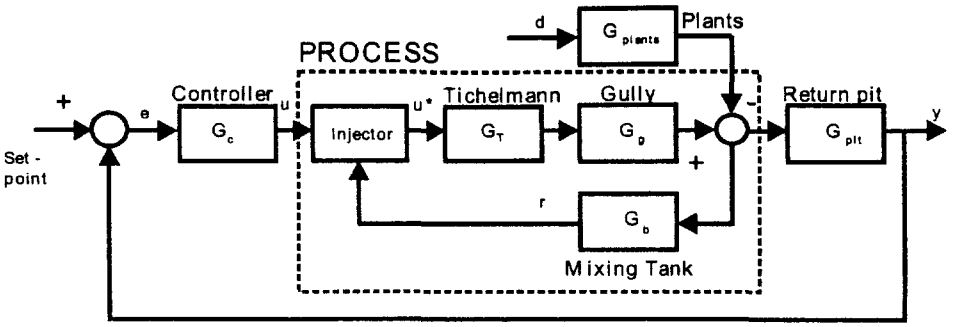


Figure 2. Diagram of the nutrient supply process with controller. $G_g$, $G_b$, $G_{pit}$, $G_t$ and $G_{plants}$ represent the transfer functions of the gully, the mixing tank, the return pit, the Tichelmann proces and the influence of the plants, respectively.

$KNO_3$ – in the main stream of the nutrient solution (Figure 1). All these parts are connected to form a closed growing system. Dead times and non-linearity's as found in the real system were used in simulations performed on the system. Dead times of appendages and pipes add together as one overall dead time. Simplifications have been made to understand better the type and shape of the overall transfer functions of some of the sub-processes.

*A model of the controlled process.*

In terms of transfer functions, the layout is shown in Figure 2. In the SISO case, which is considered here, a transfer function is defined as the quotient of the Laplace transform of the output response and its related input excitation, both as functions of time.

In this figure, $G_g$, $G_b$, $G_{pit}$, $G_T$ and $G_{plants}$ represent the transfer functions of the gully, the mixing tank, the return pit, the Tichelmann process and the influence of the plants respectively. $G_g$, $G_b$ and $G_{pit}$ are assumed to behave as first order systems. $G_c$ is the transfer function of the controller, which is subject of research and is described in this paper.

As was confirmed by simulations with a more complex model in which also non-linearity's were accounted for, the Tichelmann process can be described as a first order system, as is shown in Figure 3. Here, the dashed line is the response to a step function in the concentration at the input of the Tichelmann system. It approximates quite well the 'staircase' shaped output of the Matlab-Simulink® simulation (solid line). The staircase shape is due to the water pumped around in the supply pipes. During the first circulation cycle the water reaches the injection point with a constant concentration and it remains constant during the time it takes for the injected ions to reach the output. Each next cycle the concentration is increased at the injection point. Fluids $u$ and $r$ (Figure 2) are added each with their respective concentration. Here it needs some extra considerations.

$$\frac{Q_{pot}(t)\,X_{ion} + Q_r(t)\,X_r(t)}{Q_{pot}(t) + Q_r(t)} = X_{tich}(t) \Leftrightarrow u^*(s) = \frac{X_{ion}}{Q_{pot} + Q_r}u(s) + \frac{Q_r}{Q_{pot} + Q_r}r(s) = \alpha \cdot u(s) + \beta \cdot r(s) \quad (1)$$

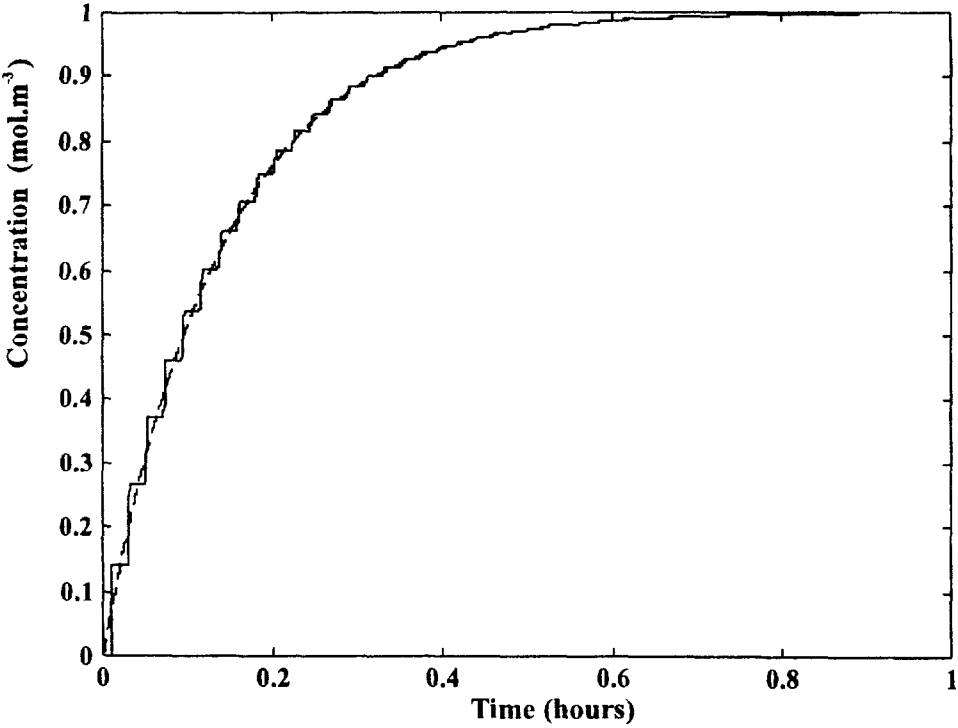


Figure 3. Step responce of potassium (solid line) and first order approximation (dashed line) of the Tichelmann system.

Equation 1 describes the actual mixing process. $Q_{pot}$ is the potassium flow ($m^3 \cdot s^{-1}$), $X_{ion}$ is the potassium concentration of the injected potassium flow ($mol \cdot m^{-3}$) and $Q_r$, $X_r$ are respectively the flowrate ($m^3 \cdot s^{-1}$) and concentration ($mol \cdot m^{-3}$) of the main-stream nutrient solution. $X_{tich}$ is the concentration of the fluid at the Tichelmann inlet. Since $Q_{pot}$ shows up in both numerators and denominators of Equation 1, this part of the process is non-linear. By stating that the potassium flow is always very small compared to the main solution flow, or $Q_{pot} << Q_r$, Equation 1 may be linearised by using $Q_{pot}$ as variable $u(s)$ in the numerator and as a small constant increment of value $Q_{pot}$ on the value of $Q_r$ in the denominator. Here, $u(s)$, $r(s)$ and $u^*(s)$ are the Laplace transform of $Q_{pot}(t)$, $X_{tich}(t)$ and $X_r(t)$ respectively. If all transfer functions are considered, the overall transfer function is of the type:

$$y(s) = \frac{\alpha \cdot G_T(s) \cdot G_g(s) \cdot G_{pit}(s) \cdot u(s) - G_{plants}(s) \cdot G_{pit}(s) \cdot d(s)}{1 - \beta \cdot G_r(s) \cdot G_g(s) \cdot G_b(s) \cdot G_{pit}(s)} \qquad (2)$$

The transfer functions used in Equation 2 are shown in Figure 2. The model in Equation 2 is the basis of the design of the controller. It should be stressed that simulations have been performed with a set of fixed flowrates of the nutrient solution in the main stream. In order to be able to cope with this kind of perturbation, the con-

troller has been designed by using the 'robust design' method (Doyle *et al.*, 1992). By using the robust design method, a whole class of system models can be controlled based on a controller that has been designed for the nominal model. Robustness in control distinguishes between robust stability and robust performance. In this particular case, the robust design method deals with uncertainties in the model description of the real process, i.e. variability of the mainstream flow and seasonal changes of the models. Loopshaping is used as a design tool for the controller. This way of designing the controller takes into account the uncertainties mentioned above and a desired performance.

*Performance and Stability*

Performance is the result of the maximum allowable difference between set point value *sp* and output *y*. From the generalised transfer diagram in Figure 4, the sensitivity function *S* is defined as the transfer from set point value *sp* to deviation *e*. Additionally a complementary sensitivity function *T* is defined as the transfer from set point value *sp* to output *y*:

$$S = \frac{1}{1 + G_c \cdot G_p} \qquad T = \frac{G_c \cdot G_p}{1 + G_c \cdot G_p} \tag{3}$$

Nominal performance is stated in terms of a weighting function $W_1$. If the performance is defined as the maximum allowable deviation between set point value and output, this performance can be reformulated as a weighting of the sensitivity function *S* by $W_1$ as in Equation 4.

Since we consider only a SISO case, the $||H||\infty$ is defined as $||H||\infty = \sup_{\omega} |H(jw)|$. Then

$$\frac{e}{sp} < \varepsilon \Leftrightarrow ||S||_\infty < \varepsilon \Leftrightarrow \left|\left|\frac{1}{\varepsilon} S\right|\right|_\infty < 1; \qquad ||W_1 \cdot S||_\infty < 1 \Rightarrow W_1 = \frac{1}{\varepsilon} \tag{4}$$

Here, instead of a performance directly related to *sp*, a performance is considered which is related to the disturbance as a result from variations in nutrient uptake by the plants. Again this performance is – indirectly – expressed as a maximum devia-

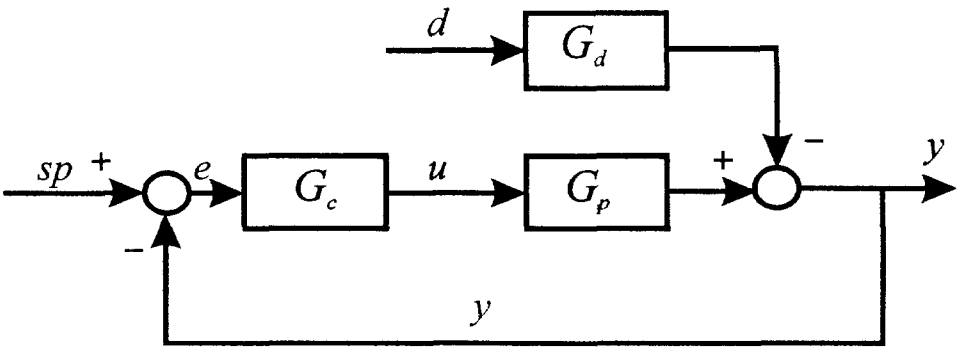


Figure 4. Generalised transfer diagram. See text for further explanation.

tion related to a set point value *sp* that is kept constant. In other words, how good will the controlled process track a (constant) *sp* when it suffers from a varying disturbance *d*. The frequency spectrum of nutrient uptake by the plants (the disturbance *d* in Figure 4) is only of interest to a maximum frequency of about $7.2 \cdot 10^{-5}$ rad·s$^{-1}$, namely one cycle of a negative cosine during a period of one day. Here, the negative cosine curve is taken as an approximation of the smoothed diurnal curve of solar radiation. Figure 4 shows the transfer from disturbance *d* to deviation *e* with constant *sp*. It is expressed as a transfer *V*, where:

$$V = \frac{G_d}{1 + G_c \cdot G_p} = G_d \cdot S \tag{5}$$

The performance requirement, chosen on the beforehand as a goal for design, states that the maximally allowable deviation from the set point value is smaller than $\varepsilon$ if disturbances are acting on the process. It introduces a new weighting function as follows:

$$\left\| \frac{1}{\varepsilon} V \right\|_\infty < 1 \Rightarrow \left\| \frac{G_d}{\varepsilon} S \right\|_\infty < 1 \Rightarrow \| \tilde{W}_1 \cdot S \|_\infty < 1 \Rightarrow \tilde{W}_1 = \frac{G_d}{\varepsilon} = W_1 \cdot G_d \tag{6}$$

Since only disturbances are considered with a frequency spectrum till $\omega_{max} = 7.2 \cdot 10^{-5}$ rad·s$^{-1}$, $\tilde{W}_1(\omega) = 0$ for $\omega > \omega_{max}$. For $\varepsilon$ the value of 0.1 was chosen. This means that maximal deviations of + or – 10% around the set point value are accepted.

A second weighting function is introduced to allow for the design of a controller *C*, that not only achieves internal stability for the nominal process, but also stabilises an entire class of models with allowable multiplicative perturbation. This class $\tilde{G}_p$ is given by :

$$\{\tilde{G}_p(s) \mid \tilde{G}_p(s) = (1 + \Delta(s) \cdot W_2) \cdot G_p(s), \|\Delta\|_\infty < 1\} \tag{7}$$

This class consists of all transfer functions $\tilde{G}_p$, such that the relative error between a perturbed model $\tilde{G}_p$ and the nominal model $G_p$ is bounded by the weighting function $W_2$, as expressed by Equation 8. A set of $\tilde{G}_p(j\omega)$ enables the determination of $W_2(j\omega)$ in Equation 8.

$$\left| \frac{\tilde{G}_p(j\omega)}{G_p(j\omega)} - 1 \right| \leq |W_2(j\omega)|, \quad \forall \omega \tag{8}$$

Then, the robust stability condition with respect to these perturbations is determined by:

$$\| W_2 \cdot T \|_\infty < 1 \tag{9}$$

*Robust Performance*

Doyle *et al.* (1992) explain the general notion of robust performance as: internal stability and performance of a specified type, which hold for all process models in $\{\tilde{G}_p\}$. The robust controller for nutrient supply is designed with an internally stable nominal feedback system, that satisfies the conditions in Equation 10. The first condition ensures the robust stability and the second condition guarantees that the closed loop system has the same performance for all perturbed process models.

$$\|W_2 \cdot T\|_\infty < 1 \text{ and } \left\| \frac{\tilde{W}_2 \cdot S}{1 + \Delta \cdot W_2 \cdot T} \right\|_\infty < 1, \ \forall \Delta \tag{10}$$

Equation 11 is a necessary and sufficient condition for the robust performance.

$$\left\| |\tilde{W}_1 \cdot S| + |W_2 \cdot T| \right\|_\infty < 1, \ \forall \Delta \tag{11}$$

Once both weighting functions are known, loopshaping is used as a tool to design the controller $C$. For this purpose the robust performance inequality in Equation 11 is rewritten as:

$$\Gamma(j\omega) = \left| \frac{\tilde{W}_1(j\omega)}{1 + L(j\omega)} \right| + \left| \frac{W_2(j\omega) \cdot L(j\omega)}{1 + L(j\omega)} \right| < 1, \ \forall \Delta \tag{12}$$

In Equation 12, $\omega$ is the frequency (rad·s$^{-1}$) and $L$ is the open loop transfer function. A Bode plot is made of both weighting functions. For all $\omega$ along the horizontal axis they should satisfy Equation 13:

$$\min\{|\tilde{W}_1|, |W_2|\} < 1, \ \forall \omega \tag{13}$$

If Equations 12 and 13 are satisfied, it can easily be seen that both the nominal performance (Equation 6) and robust stability (Equation 9) are ensured. Equation 12 implies, that at a certain frequency an improved nominal performance ($\tilde{W}_1$ is large) entails a decreased robustness ($W_2$ is large) and vice versa, because both $\tilde{W}_1$ and $W_2$ can not be large at the same frequency.

The loopshaping process now consists of finding a transfer function $L$ in the Bode diagram, that fulfils the inequalities in Equation 12. In order to ease this process, it should be noted that these constraints mean, that in general Equations 14 and 15 should hold in the high and in the low frequency range respectively.

$$|\mathrm{L}| < \frac{1 - |\tilde{W}_1|}{|W_2|} \tag{14}$$

$$|\mathrm{L}| > \frac{|\tilde{W}_1|}{1 - |W_2|} \tag{15}$$

Now an $L$, which satisfies the inequalities in Equations 14 and 15, is chosen in such a way that the inequality in Equation 12 holds. Since in Figure 4 $L = G_c G_p$ and $G_p$ is known, $G_c$ can be calculated. However, in the specific approach described here, $G_c$ rather than $L$ is calculated directly for reasons to have some influence on the complexity of the controller.

## Results and discussion

### *Weighting function* $\tilde{W}_1$

Weighting function $\tilde{W}_1$ can be determined only if the transfer function from disturbance $d$ to $y$ is known (Figure 4). A simulation with the Simulink® model of the

process produced the transfer function $G_d$. By analysing the Simulink® model and after some minor simplifications it could be shown that the transfer function from $d$ to $y$ was of the form as in Equation 16. Since the form of the transfer function was known it was sufficient to fit the parameters in Equation 16 on the basis of step responses of the disturbance $d$ in the Simulink® model, with constant input $u$. Five simulations were carried out for the following set of pairs of disturbance $d$ and drain flow $r$: {( $7.5 \cdot 10^{-5}$ $m^3 \cdot s^{-1}$, nominal), ($1.5 \cdot 10^{-4}$ $m^3 \cdot s^{-1}$, nominal + 10%), ($1.5 \cdot 10^{-4}$ $m^3 \cdot s^{-1}$, nominal – 10%), (0, nominal + 10%), (0, nominal – 10%)}.

$$G_d(s) = \frac{A \cdot s^2 + B \cdot s + C}{D \cdot s^4 + E \cdot s^3 + F \cdot s^2 + s} \tag{16}$$

It resulted in a series of five values for A through F as in Table 1.

Table 1. Parameter values of $G_d(s)$ as in Equation 16.

| Simultation run | Parameter | | | | | |
|---|---|---|---|---|---|---|
| | A | B | C | D | E | F |
| 1 | $4.83 \cdot 10^{2}$ | $5.49 \cdot 10^{-1}$ | $1.16 \cdot 10^{-4}$ | $6.32 \cdot 10^{9}$ | $1.03 \cdot 10^{7}$ | $5.55 \cdot 10^{3}$ |
| 2 | $5.61 \cdot 10^{2}$ | $8.22 \cdot 10^{-1}$ | $2.49 \cdot 10^{-4}$ | $3.32 \cdot 10^{9}$ | $6.67 \cdot 10^{6}$ | $4.47 \cdot 10^{3}$ |
| 3 | $7.55 \cdot 10^{2}$ | $9.46 \cdot 10^{-1}$ | $2.54 \cdot 10^{-4}$ | $5.44 \cdot 10^{9}$ | $9.28 \cdot 10^{6}$ | $5.28 \cdot 10^{3}$ |
| 4 | $1.37 \cdot 10^{2}$ | $2.43 \cdot 10^{-6}$ | $1.08 \cdot 10^{-10}$ | $1.21 \cdot 10^{11}$ | $9.02 \cdot 10^{7}$ | $1.94 \cdot 10^{4}$ |
| 5 | $9.25 \cdot 10^{2}$ | $1.99 \cdot 10^{-6}$ | $1.08 \cdot 10^{-10}$ | $1.00 \cdot 10^{11}$ | $6.81 \cdot 10^{7}$ | $1.46 \cdot 10^{4}$ |

Equation 16 and the five simulation runs produced five different $\tilde{W}_1$ functions. In order to choose the best function for $\tilde{W}_1$, $|\tilde{W}_1(j\omega)|$ was calculated for all five simulations and depicted in a Bode plot (Figure 5a). The upper line (simulation run 2) exceeds the other four lines, thus satisfying best the conditions of Equation 13. Inspection of the diagram of simulation run 2 of the Bode plots in Figure 5b revealed, that the transfer function of $\tilde{W}$ could be reduced to the much more simpler form:

$$\tilde{W}_1 = \frac{2.7 \cdot 10^{-3}}{1.3 \cdot 10^{-3} \cdot s^2 + s} \tag{17}$$

Since the reduced form still encloses the Bode plots of the other five functions (Figure 5b), it was used to continue the loopshaping process. The second weighting function $W_2$ takes into account the perturbations of the nominal model. The nominal model will be perturbed as a result of dynamics in the flows.

All flows were related to the three most important flows, i.e. the potassium injection flow, the nutrient solution flow due to plant uptake and the drain flow. These three flows had $2^3 = 8$ combinations of upper and lower boundaries, which had to be taken into account in the same type of simulation-fit procedure as described before for the $\tilde{W}_1$ weighting function, however, now with a step function on $u$ and a constant value for $d$.

The $W_2$ weighting function was determined by Equation 8. The set of transfer functions $\tilde{G}_p$ were found to be of the type as in Equation 18:

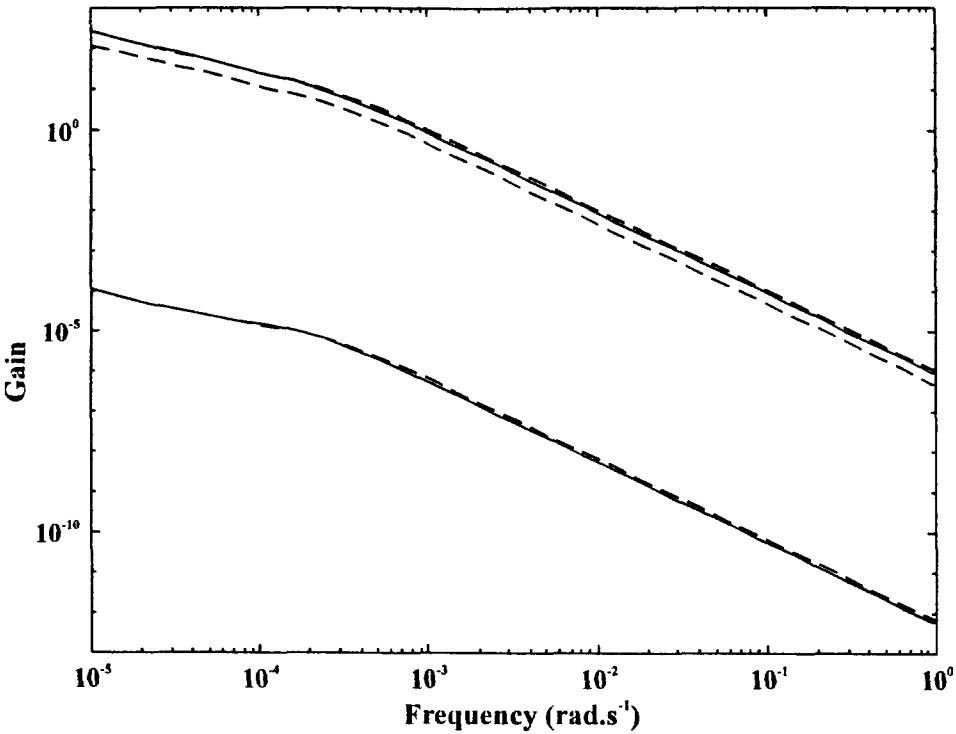


Figure 5a. Weighting function $\tilde{W}_1$ run 2,3,1,4 and 5 counting from above, respectively.

$$\tilde{G}_p = \frac{A \cdot s + B}{C \cdot s^4 + D \cdot s^3 + E \cdot s^2 + s} \tag{18}$$

The simulation procedure together with Equations 8 and 18 produced eight series of parameters A through E. The resultant eight Bode plots for $|(\tilde{G}_p \cdot G_p^{-1}) - 1|$ are depicted in Figure 6a. The function values (for all $\omega$) represented by the dashed line in Figure 6a exceed the values of all simulation outputs and thus – according to the constraint in Equation 8 – is a sufficient representation of the weighting function in Equation 19:

$$W_2 = \frac{2.29 \cdot 10^5 \cdot s^2 + 2.21 \cdot 10^3 \cdot s + 3.03 \cdot 10^{-1}}{1.08 \cdot 10^5 \cdot s^2 + 2.74 \cdot 10^3 \cdot s + 1} \tag{19}$$

Since step functions were used for the excitation of the system – and step functions do not give much insight in the high frequency properties of a system under test – the last part of the $W_2$ function (dashed line in Figure 6b) was kept at a relatively large distance from the upper-most of the eight graphs.

Now $\tilde{W}_1$ and $W_2$ were known and the controller could be determined by means of 'loopshaping'. For this purpose $L = G_p \cdot G_c$ was used. Now, $G_p$ is known and $G_c$ is chosen to determine $L$ in such a way, that inequalities in Equation 14 and 15 were satis-

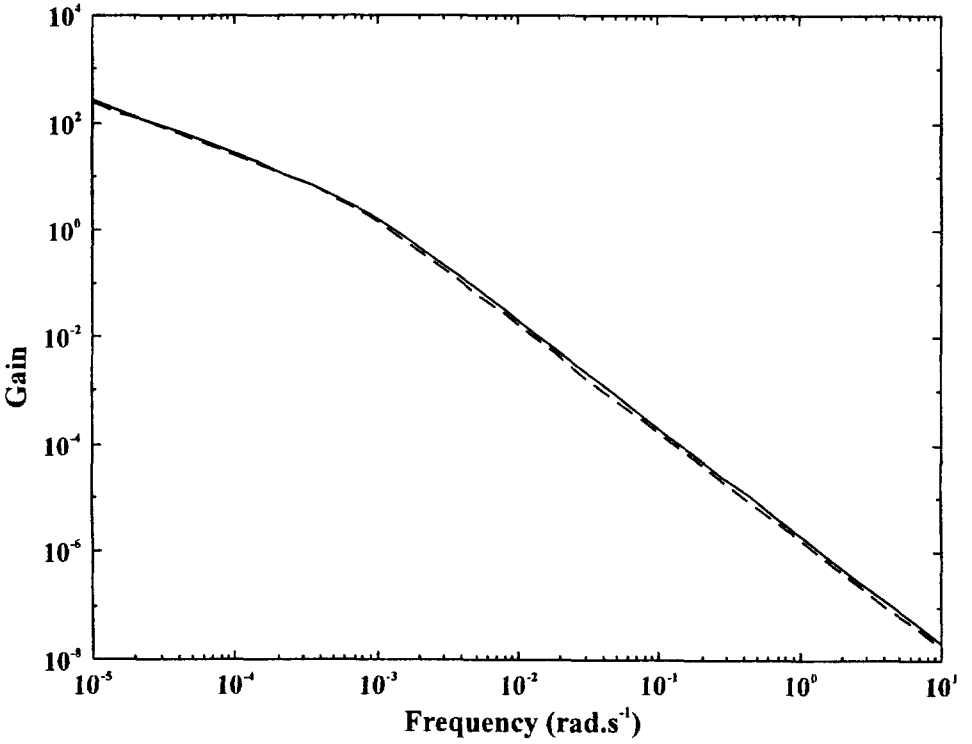


Figure 5b. Reduced form (solid) and $\tilde{W}_1$ for run 2 (dashed).

fied for the high and low frequency range respectively. Halfway through the frequency range the shape of $L$ could be chosen freely, as long as Equation 12 was satisfied. Finally, it produced the controller transfer function, that satisfied all constraints as depicted in Equation 20 with an $|L|$ as in Figure 6b (solid).

$$G_c(s) = \frac{5.92 \cdot 10^2 \cdot s^3 + 5.15 \cdot s^2 + 1.18 \cdot 10^{-2} \cdot s + 2.9 \cdot 10^{-6}}{2.62 \cdot 10^5 \cdot s^3 + 1.23 \cdot 10^4 \cdot s^2 + 1.92 \cdot s + 1} \qquad (20)$$

*Test of the control algorithm*

A simulation test of the control algorithm was performed with a simulation set-up as is shown in Figure 7. The results are presented in Figure 8.

A unit step was applied to simulate *sp*. From the tenth hour onwards a negative cosine was applied, as a disturbance acting on the process, with a mean value of 5.7 mol·s$^{-1}$, mimicking the nutrient uptake by the plants.

The process in Figure 7 is a Matlab-Simulink* model of the controlled system. Three different flowrates (minimum, nominal and maximum) were simulated for the potassium pump, the plant uptake and the gully. The extreme values of the flowrates induce the maximum expected perturbation of the model. In Figure 8, curve (a) is

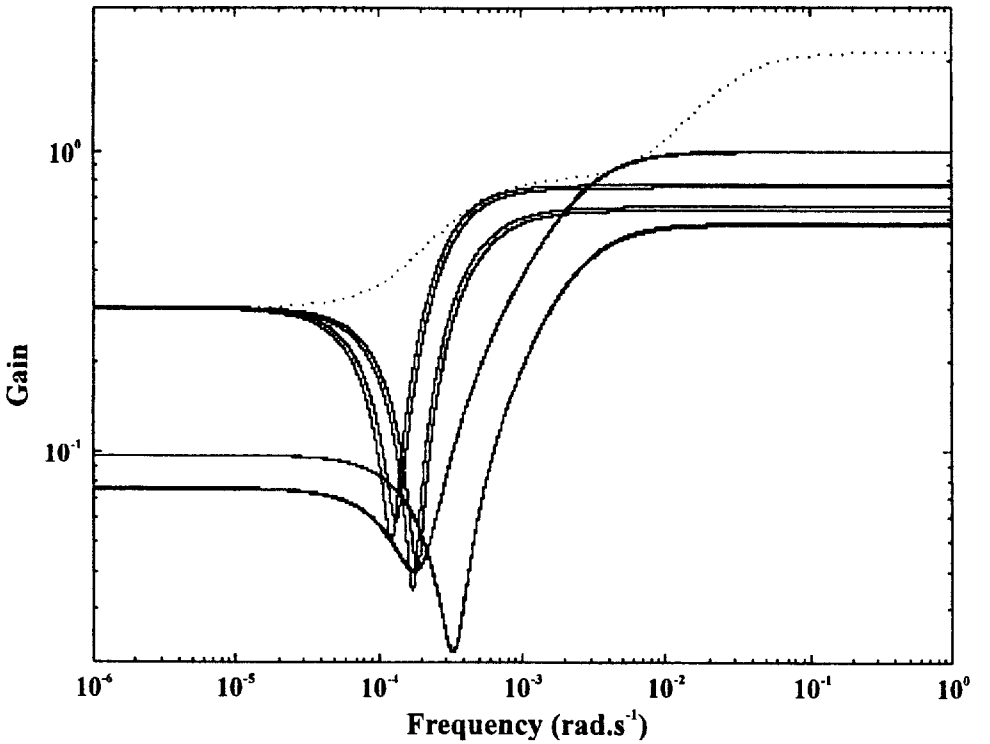


Figure 6a. Results of the eight simulation runs (solid) and of $\tilde{W}_2$ function (dots).

the response with nominal flowrates, curve (b) is the response with high flowrates and curve (c) is the response with low flowrates. Curve (d) shows the simulated flow through the potassium injection pump and shows the compensation for the unit step in the first hours and for the negative cosine of plant uptake from the tenth hour onwards. All three simulation results a) through c) show almost no residue of the disturbance in the output signal, hence the controller is able to keep the maximum deviation well within the indicated allowable margin of 10%.

*Preparing the controller for implementation*

The system under test was implemented as a Direct Digital Controller, using a SCADA measurement and control system. The smallest time period between samples of measured data was 6.4 seconds. The same time was needed for the control actions to be effective at the valves and pumps. To implement the control algorithm in a Direct Digital Controller, the continuous time transfer function $G_c$ of Equation 20 was transformed into a discrete time transfer function. First, the continuous time transfer function was transformed into a state space system (Equation 21).

In Equation 21 variables $x(t)$, $y(t)$ and $u(t)$ are the state variable, output and input

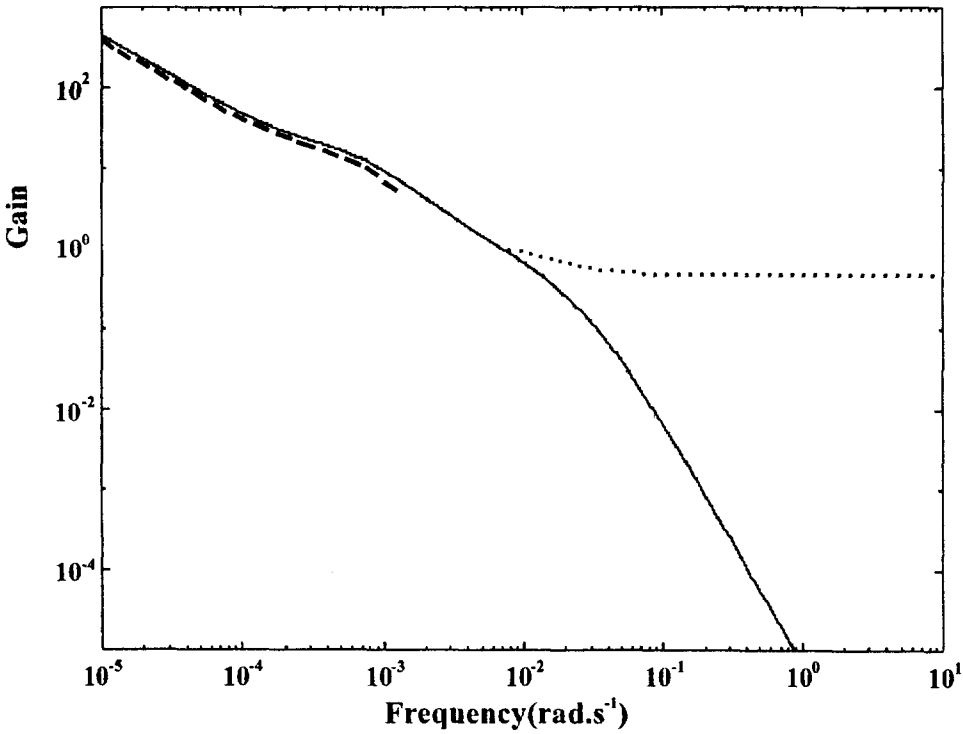


Figure 6b. Diagram shows $|L|$ (solid) and its limits in the upper (dots and lower (dashed) frequency area.

of the controller respectively, A, B, C and D are system matrices, the values of which are given in Equation 22.

$$\dot{x}(t) = A \cdot x(t) + B \cdot u(t)$$
$$y(t) = C \cdot x(t) + D \cdot u(t) \qquad (21)$$

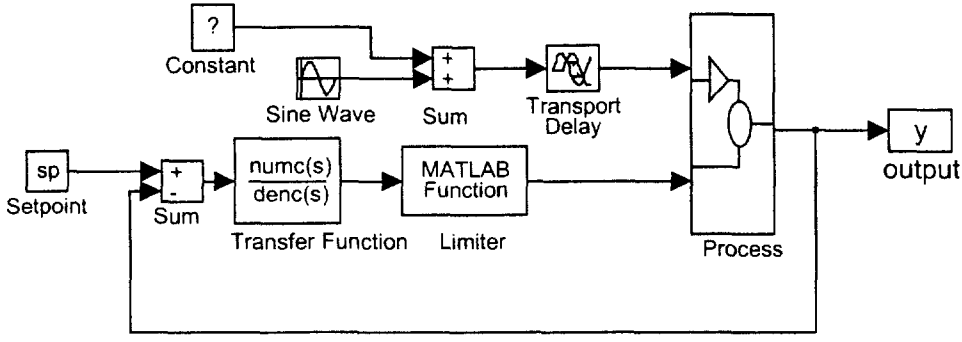


Figure 7. The controlled system in Matlab Simulink®.

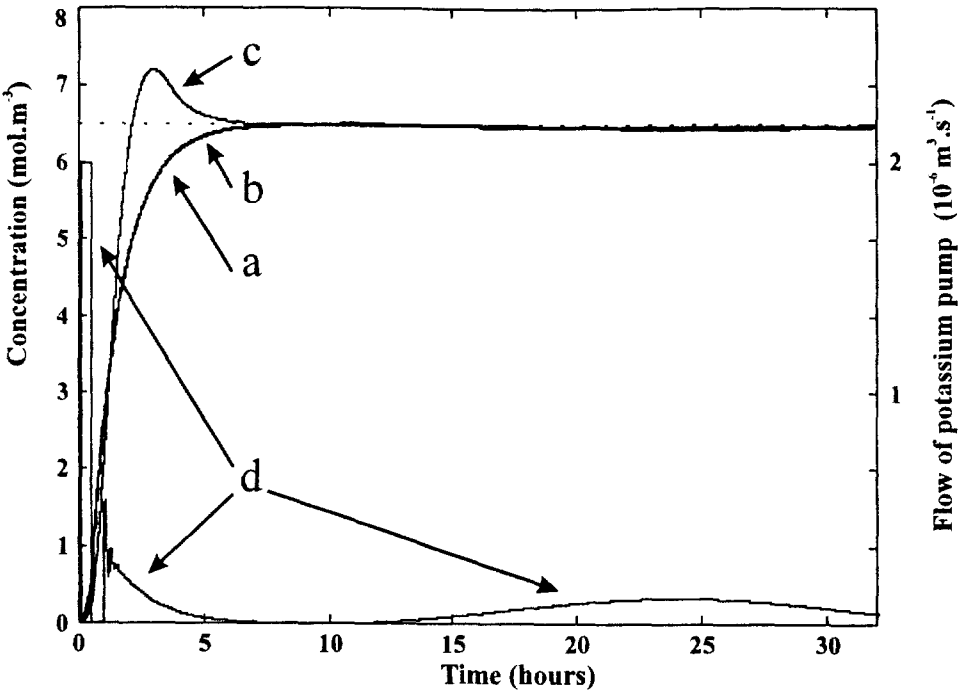


Figure 8. Simulation results at nominal flowrates (a), at low flowrates (b), at hight flowrates (c) and nutrient injection at nominal flowrate (d).

$$A = \begin{bmatrix} -4.7\cdot10^{-2} & -7.3\cdot10^{-4} & -3.8\cdot10^{-6} \\ 1 & 0 & 0 \\ 0 & 1 & 0 \end{bmatrix}; B = \begin{bmatrix} 1 \\ 0 \\ 0 \end{bmatrix}; C^T = \begin{bmatrix} -8.6\cdot10^{-5} \\ -1.6\cdot10^{-6} \\ -8.6\cdot10^{-9} \end{bmatrix}; D = 2.3\cdot1^{-3} \quad (22)$$

The discrete time version of the controller transfer is depicted in Equation 23. $A_d$, $B_d$, $C_d$ and $D_d$ in Equation 23 are the discrete time system matrices. A Matlab® procedure is used to transform the continuous time system matrices (Equation 22) into discrete system matrices (Equation 24). The Matlab® Control Toolbox, which is connected to the SCADA system, directly accepts the matrices of Equation 24 to control the real process.

$$\begin{aligned} x((n+1)\cdot T) &= A_d\cdot x(n\cdot T) + B_d\cdot u(n\cdot T) \\ y(n\cdot T) &= C_d\cdot x(n\cdot T) + D_d\cdot u(n\cdot T) \end{aligned} \quad (23)$$

$$A_d = \begin{bmatrix} 6.0\cdot10^{-1} & -5.9\cdot10^{-3} & -3.0\cdot10^{-5} \\ 7.9 & 9.7\cdot10^{-1} & -1.6\cdot10^{-4} \\ 42.8 & 9.9 & 1 \end{bmatrix}; B_d = \begin{bmatrix} 7.9 \\ 42.8 \\ 148 \end{bmatrix}; C_d^T = \begin{bmatrix} -8.6\cdot10^{-5} \\ -1.6\cdot10^{-6} \\ -8.6\cdot10^{-9} \end{bmatrix}; D_d = 2.3\cdot10^{-3} \quad (24)$$

The simulation data showed that the dynamics in the nutrient supply process were more complicated than was expected at a first glance. More standard design proce-

dures (PI, PID etc.) could lead to a stable controlled process, but would certainly be more conservative than the robust controller presented.

As was shown, robust control solves problems if a model of the process contains uncertainties. It keeps the performance of a controlled process within pre-set limits. Robust performance and robust stability – as qualities of the controlled process – were shown to be feasible for the control of nutrient application in closed growing systems. Loopshaping as a design tool gave a lot of insight into the process and its control. It did help the engineer to find his way around design pitfalls. Especially in this application, the loopshaping method resulted in a controller, which met the desired performance, despite the uncertainties in the process. It showed to be a straight forward design procedure, useful for non-specialists with the aid of some mathematical toolboxes.

A simulation test showed very good results in terms of disturbance suppression of the controlled process: the response on an excitation with a negative cosine disturbance stayed well within the pre-set 10% limits. The response corresponding to input excitation showed that the controller did not perform very well for set value tracking, but – as was stated in the introduction – this was clearly not intended at the start of the design.

**Acknowledgement**

The authors wish to thank the EU AIR III Research Program and the Ministry of Agriculture Nature Management and Fisheries of the Netherlands for the sponsoring of this research project.

## References

Chotai, A. & P.C. Young, 1991. Self-adaptive and self-tuning control of a Nutrient Film System. In: Hashimoto Y. & W. Day (Eds.), Mathematical and Control Applications in Agriculture and Horticulture. Pergamon Press, Oxford, pp. 33–40.

Chotai, A., P.C. Young, P. Davis & Z.S. Chalabi, 1991. True digital control of glasshouse systems. In: Hashimoto Y. & W. Day (Eds.), Mathematical and Control Applications in Agriculture and Horticulture. Pergamon Press, Oxford, pp. 41–46.

Doyle, J.C., B.A. Francis & A.R. Tannenbaum, 1992. Feedback control theory. Maxwell Macmillan International Editions, New York, 227 pp.

Gieling, T.H., J. Bontsema, A.W.J. van Antwerpen & L.J.S. Lucasse, 1994. Monitoring and control of water and fertilizer distribution in greenhouses. *Acta Horticulturae* 401: 365–372.

Gieling, T.H., H.H. van den Vlekkert, 1996. Application of ISFETs in closed loop systems for greenhouses. *Adv. Space Res.* 18, no. 4/5, pp. 135–138.

Hashimoto, Y., T. Morimoto, T. Fukuyama, H. Watake, S., Yamaguchi & H. Kikuchi, 1989. Identification and control of hydroponic system using ion sensors. *Acta Horticulturae* 245: 490–497.

Honjo, T. & T. Takakura, 1991. Identification of water and nutrient supply to hydroponic tomato plants by using neural nets. In: Hashimoto Y. & W. Day, Mathematical and Control Applications in Agriculture and Horticulture. Pergamon Press, Oxford, pp. 285–288.

Kupers, G., J. van Gaalen., T.H. Gieling & E.A. van Os, 1992. Diurnal changes in the ion concentration of the supply and return water of a tomato crop grown on rockwool. *Acta Horticulturae* 304: 291–300.

Okuya A. & T. Okuya, 1991. Development of an ion controlled feeding method in hydroponics. In: Hashimoto Y. & W. Day (Eds.), Mathematical and Control Applications in Agriculture and Horticulture. Pergamon Press, Oxford, pp. 355–360.

Young P.C., Tych W. & Chotai A., 1991. Identification, estimation and control of glasshouse systems. In: Hashimoto Y. & W. Day (Eds.), Mathematical and Control Applications in Agriculture and Horticulture. Pergamon Press, Oxford, pp. 307–317.